

Electronic Supplementary Material (ESI) for Nanoscale  
This journal is © The Royal Society of Chemistry 2012

## Electronic Supplementary Information

# Hydrogen bonding-driven rheological modulation of **chemically reduced graphene oxide**/poly(vinyl alcohol) suspensions and its application in electrospinning

Yeqiang Tan, Yihu Song\*, and Qiang Zheng

**Experiment section** (S3-S4)

**Fig. S1** UV-Vis spectra of 0.1 mg mL<sup>-1</sup> GO and **RGO** aqueous dispersions. (S5)

**Fig. S2** XPS spectra of GO and **RGO** powders. (S5)

**Fig. S3** Raman spectra of GO and **RGO** powders. (S6)

**Fig. S4** XRD patterns of pristine graphite, GO, **RGO**, PVA film and the nanocomposite films containing 1 wt% nanosheets. (S6)

**Fig. S5** OM micrographs of 1 wt% GO/PVA (A) and **RGO**/PVA (B) suspensions. Insets show photographs of GO and **RGO** suspensions placed statically for around 2 months. (S7)

**Fig. S6** Schematic illustration of the ordered structure of **RGO** sheets in the in-situ shear flow capillary cell. (S7)

**Fig. S7** (A) Storage modulus ( $G'$ ) as a function of strain ( $\gamma$ ) for PVA solution ( $C = 10$  wt%) and the GO/PVA (hollow symbols) and **RGO**/PVA suspensions (solid symbols) at 3.14 rad s<sup>-1</sup> at 20 °C. (B) Critical strain ( $\gamma_c$ ) and  $G'$  in the linearity region ( $G'_0$ ) as a function of GO or **RGO** loading. (S8)

**Fig. S8** (A) Storage modulus ( $G'$ ) and (B) loss modulus ( $G''$ ) as a function of frequency ( $\omega$ ) for PVA solution ( $C = 10$  wt%) and the GO/PVA (hollow symbols) and **RGO**/PVA suspensions (solid symbols) at 5 °C. (S8)

**Fig. S9** (A) Storage modulus ( $E'$ ) and (B) loss fact ( $\tan\delta$ ) as a function of temperature ( $T$ ) for PVA, GO/PVA and **RGO**/PVA films; (C)  $T_g$  and  $E'$  at 25 °C as a function of fillers loading. (S9)

**Fig. S10** The peak hold curves of various spinning solutions. (S9)

**Fig. S11** Size distribution histograms of GO/PVA nanofiber electrospun at  $C = 5$  wt% calculated from Fig. 11A2 (A) and of **RGO**/PVA nanofiber electrospun at  $C = 18$  wt% calculated from Fig. 11B2 (B) with the aid of Image J. The red curve is drawn according to Gaussian distribution. (S10)

**Table S1. Rheological exponents for PVA solution ( $C = 10$  wt%) and nanosheet suspensions.** (S11)

**Table S2. Viscosity values of spinning solutions and structural parameters of corresponding fibers.** (S11)

**Reference** (S12)

## Experiment section

### Materials

Graphite (99.8%) with an average particle size of 45  $\mu\text{m}$  was obtained from Alfa Aesar Co. Ltd., UK. Concentrated sulfuric acid ( $\text{H}_2\text{SO}_4$ ), concentrated hydrochloric acid (HCl), potassium persulfate ( $\text{K}_2\text{S}_2\text{O}_8$ ), phosphorus pentoxide ( $\text{P}_2\text{O}_5$ ), potassium permanganate ( $\text{KMnO}_4$ ), sodium nitrate ( $\text{NaNO}_3$ ), hydrogen peroxide ( $\text{H}_2\text{O}_2$ , 30%), and hydrazine hydrate (85%) were purchased from Shanghai Chem. Reagent Co. Ltd., China. PVA ( $M_w$  108 000, 98–99% hydrolysed) was purchased from Sinopharm Chem. Reagent Co. Ltd., China. All the materials were used without further purification.

### Preparation of graphene oxide and chemically reduced graphene oxide nanosheets

Graphene oxide (GO) was synthesized from natural graphite powder using a modified Hummers' method<sup>1,2</sup> including two steps of oxidation. In the pre-oxidation step,  $\text{K}_2\text{S}_2\text{O}_8$  (8.4g) and  $\text{P}_2\text{O}_5$  (8.4 g) were dissolved in concentrated  $\text{H}_2\text{SO}_4$  (40 mL) at 80 °C, followed by slow addition of graphite powder (10 g). The oxidation reaction was conducted at 80 °C for 4.5 h. After cooling down to room temperature, the suspension was diluted with deionized water and laid overnight. The mixture was then vacuum-filtered and washed with deionized water (1.5 L) using a 0.22  $\mu\text{m}$  polycarbonate membrane. The product obtained was dried in air at room temperature. In the second oxidation step, the pretreated graphite powder was poured into concentrated  $\text{H}_2\text{SO}_4$  (230 mL) in an ice bath and stirred until the temperature dropped to 0–3 °C.  $\text{KMnO}_4$  (60 g) was added gradually under continuous stirring, and the temperature was kept below 10 °C. The mixture was then heated to 35 °C and stirred for 2 h, followed by diluting with deionized water (0.5 L) and further stirring for 30 min. The reaction was terminated by adding deionized water (1.5 L) and 30 %  $\text{H}_2\text{O}_2$  (25 mL). The mixture was left undisturbed for 2 days and the nearly clear supernatant was decanted. The lower precipitate was filtered and washed with 1 M HCl solution to remove residual metal oxides. The products were subjected to cycles of water-washing and separation via centrifugation until pH value of the decantate reached 6. The sample of GO was obtained after freeze-dehydration for 2 days. **Chemically reduced graphene oxide (RGO)** was synthesized from the as-prepared GO sheets. The GO product (50 mg) was suspended in deionized water (100 mL) to create a yellow-brown dispersion by sonication for 30 min. The suspension was mixed with hydrazine (40  $\mu\text{L}$ ) as a reducing agent, and ammonia (200  $\mu\text{L}$ ) as a stabilizer was added to adjust pH to around 10. After being magnetically stirred for a few minutes, the suspension was refluxed at 95 °C for 24 h. The product was vacuum-filtered through a 0.22  $\mu\text{m}$  polytetrafluoroethylene membrane and was washed with deionized water and methanol. **RGO** was obtained after vacuum-drying for 24 h.

### Preparation of GO/PVA and RGO/PVA suspensions

A typical preparation procedure for GO/PVA suspensions with GO loadings of 0.5, 1 and 1.5 wt% with respect to PVA content was as follows. Certain amounts of GO powder were dispersed in deionized water and treated with ultrasound for 30 min, yielding completely exfoliated GO sheet suspension.<sup>22</sup> PVA powder was dissolved in deionized water at 95 °C for 2 h and the solution was subsequently cooled down to room temperature. The GO dispersion was gradually added to the PVA solution under magnetic agitation and was sonicated for an additional 30 min to obtain GO/PVA suspensions. To prepare **RGO/PVA** suspensions, hydrazine was added to the as-prepared GO/PVA suspensions under magnetic agitation for 30 min. GO were reduced to **RGO** by refluxing the mixture at 95 °C for 24 h. The presence of PVA molecular chains effectively retarded the aggregation of **RGO** sheets during the reduction reaction.<sup>3</sup> The GO loading before reduction was regarded as the **RGO** loading in the **RGO/PVA** suspensions for facile comparison. Particularly, different reduction times (3, 10, 20 min, and 1, 2, 6, and 24 h) were adopted in preparing suspensions with 1 wt% **RGO**. The suspensions were poured onto a glass plate and kept at 60 °C for film formation until constant weights. The films were peeled off for modulated differential scanning calorimeter (MDSC) and dynamic mechanical analysis (DMA).

### Electrospinning process

After air bubbles were removed completely, the prepared PVA solution, GO/PVA and **RGO/PVA** suspensions were poured into a 20 mL syringe bearing a 0.7 mm inner diameter metal needle which was connected with a high voltage power supply (GDW-a, Tianjin Dongwen High-voltage Power Supply Plant, China). The grounded counter electrode was covered with an aluminum foil collector. Typically, electrospinning was performed at 18 kV voltage, 12 cm distance between the needle tip and the ground electrode. The flow rate of the solution was controlled at 0.5 mL h<sup>-1</sup> by a syringe pump (WZ-50C2, Zhejiang University Medical Instrument Co. Ltd., China). All electrospinnings were conducted at room temperature (25 °C) in an enclosed chamber, in which the relative humidity could be controlled at 50% by dehumidifier/steam humidifier.

### Characterizations

Atomic force microscopy (AFM) tapping-mode images were taken on NSK SPI3800 (NSK Co. Ltd., Japan). The samples were prepared by spin-coating the solutions onto freshly exfoliated mica substrates. X-ray diffraction (XRD) was carried out using a Rigaku X-ray generator equipped with Cu K $\alpha$  radiation ( $\lambda = 0.154$  nm) (Rigaku Co. Ltd., Japan). X-ray photoelectron spectroscopy (XPS) was recorded on a PHI 5000c ESCA photoelectron spectrometer (PHI, USA) to detect C/O atomic ratios of GO and **RGO** powders. Raman spectra were collected on an ALMEGA-Dispersive Raman (Thermo Nicolet, USA) with a 514.5 nm excitation. The UV-Vis absorption spectra were measured on a Lambda 35 spectrophotometer (Perkin-Elmer, USA). The dispersity at the static state and the ordering under

intensive shear flow for GO and RGO sheets was demonstrated by polarized-light optical microscopy (POM) equipped with a camera (Nikon E600POL, Japan) under different mode. The suspensions were loaded into the capillary cells, and the flow field was applied by the syringe pump with flow rate of  $3.0 \text{ mL h}^{-1}$ . Rheological measurements were carried out on an advanced rheometer (AR-G2, TA Instruments, USA) with parallel plate grippers of 40 mm in diameter. The gap distance was kept about 0.5 mm for all tests. All the samples were presheared at  $0.1 \text{ s}^{-1}$  for 1 min to unify the shear history. Steady flow tests were performed in the strain rate range of 0.01 to  $1000 \text{ s}^{-1}$ . Strain sweeps from 0.1 % to 1000 % were conducted at  $3.14 \text{ rad s}^{-1}$  to determine the linear region. Dynamic frequency ( $\omega$ ) sweeps were performed from 0.1 to  $10^2 \text{ rad s}^{-1}$  under 0.5 % strain amplitude in the linearity region. Fourier-transform infrared/attenuated total reflectance (FT-IR/ATR) spectroscopy were collected using Nicolet FT-IR/Nexus470 spectrometer (USA) equipped with an ATR accessory (ZnSe crystal,  $45^\circ$ ). Sixteen scans were taken for each spectrum at a nominal resolution of  $2 \text{ cm}^{-1}$ . Thermograms were recorded using a Q100 differential scanning calorimeter (DSC, TA, USA), which was calibrated using indium. The ice-melting enthalpies of PVA solution and suspensions were measured in standard mode to determine hydration number of PVA chains in aqueous solution. The sealed sample pan was placed in the calorimeter instrument and cooled to  $-40 \text{ }^\circ\text{C}$  to freeze the solution and was then heated from  $-40 \text{ }^\circ\text{C}$  to  $40 \text{ }^\circ\text{C}$  at a heating rate of  $5 \text{ }^\circ\text{C min}^{-1}$  for avoiding the time lag of response caused by a faster heating rate. The thermal behaviors of nanocomposite films were measured in the modulation mode. Firstly, the samples were heated to  $100 \text{ }^\circ\text{C}$  and held for 5 min to unify the heat history of different samples. Subsequently, the samples were heated from  $-30 \text{ }^\circ\text{C}$  to  $240 \text{ }^\circ\text{C}$  at  $3 \text{ }^\circ\text{C min}^{-1}$  with an amplitude of  $1 \text{ }^\circ\text{C}$  and a period of 60 s. Dynamic mechanical analysis (DMA) was conducted on Q800 (TA, USA) in tensile mode at  $\omega = 1 \text{ Hz}$ . The samples were heated from  $-30 \text{ }^\circ\text{C}$  to  $160 \text{ }^\circ\text{C}$  at a heating rate of  $3 \text{ }^\circ\text{C min}^{-1}$ . For electrospinning process, the solution viscosity was measured with AR-G2 under the mode of peak holding at a certain shear rate. The fibrous morphology was observed under a scanning electron microscope (SEM, S4800, Hitachi, Japan) at an acceleration voltage of 3 kV. Transmission electron microscope (TEM, JEM-1200EX, JEOL, Japan) was employed to investigate the dispersity and the ordering of GO or RGO by depositing electrospun nanofibers directly onto TEM Cu slot grids. The average fibrous diameter was calculated from the SEM pictures with the aid of computer software (ImageJ Version 1.45). Thermal stability of the nanofibers was evaluated by thermogravimetry analysis (TGA, Q1000, TA, USA) at a heating rate of  $10 \text{ }^\circ\text{C min}^{-1}$  under nitrogen.

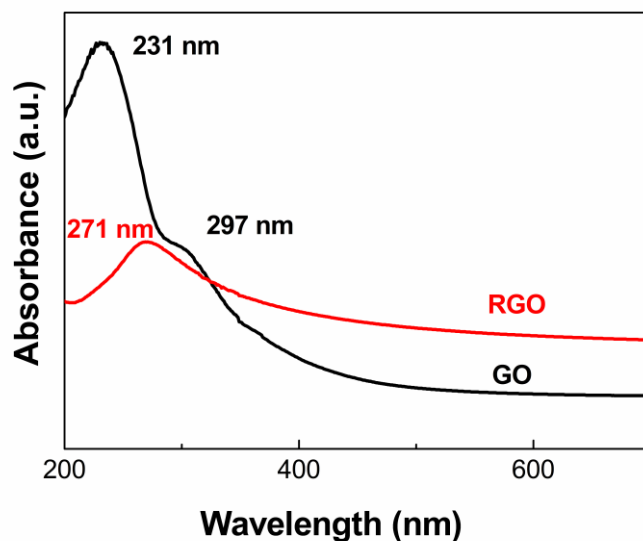


**Fig. S1** UV-Vis spectra of 0.1 mg mL<sup>-1</sup> GO and RGO aqueous dispersions. The UV-Vis curve of GO dispersion exhibits a peak at 231 nm and a shoulder at 297 nm, attributed to  $\pi \rightarrow \pi^*$  transition of phenyl and  $n \rightarrow \pi^*$  transition of C=O bonds, respectively. For the RGO, the characterized peak at 231 nm red-shifts to 271 nm due to the restored electronic conjugation upon reduction, which is in agreement with previous reports.<sup>4</sup>

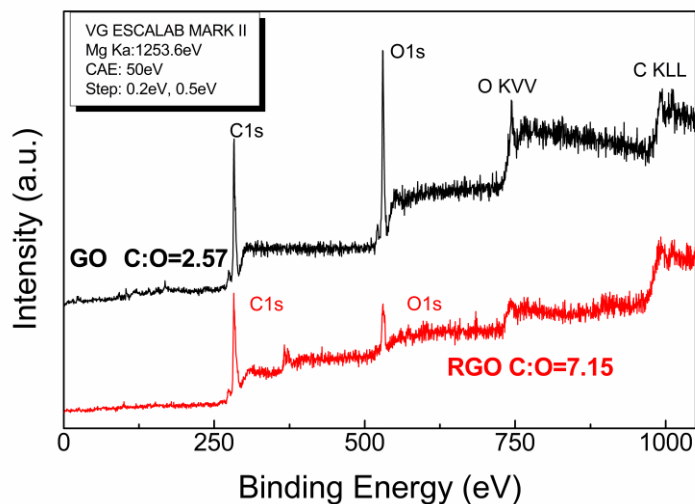


**Fig. S2** XPS spectra of GO and RGO powders. XPS can quantitatively characterize oxidation degree of GO and the reduction degree of RGO. The C/O atomic ratio (2.57) of GO is much lower than that (20.7) of pristine graphite,<sup>3</sup> confirming the heavy oxidation in GO. Meanwhile, the C/O atomic ratio (7.15) of RGO is much higher than that of GO, suggesting that the hydrazine reduction can effectively remove majority of oxygen-containing groups on GO sheets.

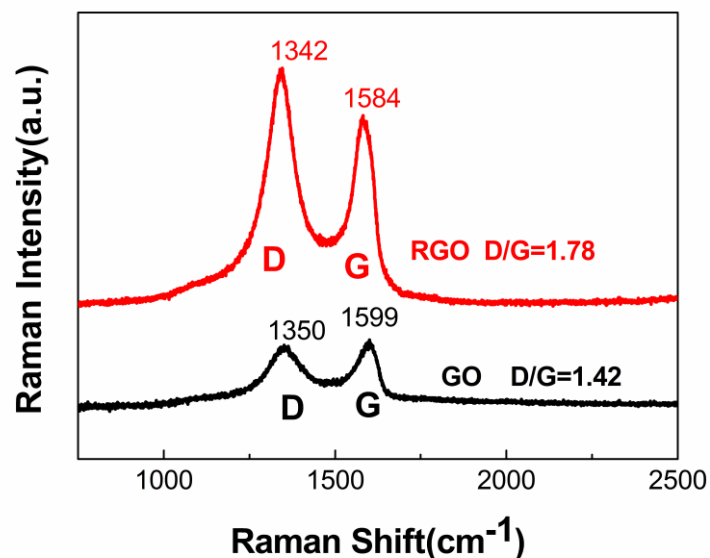


**Fig. S3** Raman spectra of GO and **RGO** powders. The two fundamental Raman peaks at  $1599\text{ cm}^{-1}$  (G band) and  $1350\text{ cm}^{-1}$  (D band) of GO are attributed to the vibration of  $sp^2$ -hybridized graphitic domains and structural defects (disorder-induced modes), respectively.<sup>5</sup> After reduction, the G and D bands move to  $1584\text{ cm}^{-1}$  and  $1342\text{ cm}^{-1}$ , respectively, which are close to the values of pristine graphite and indicate the production of **RGO** after hydrazine treatment. Fitting of the Raman spectra gives the D/G intensity ratios of 1.78 and 1.42, respectively, for **RGO** and GO, suggesting more  $sp^2$  domains of smaller size or highly defected carbon lattices formed during the reduction of GO, which agrees well with several studies.<sup>6</sup>

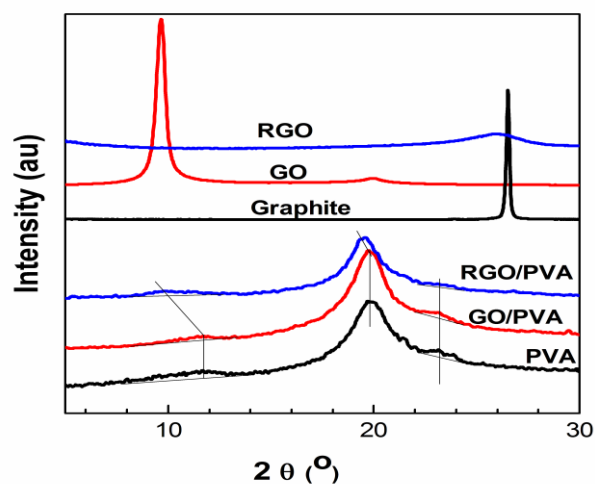


**Fig. S4** XRD patterns of pristine graphite, GO, **RGO**, PVA film and the nanocomposite films containing 1 wt% nanosheets. Pristine graphite exhibits a sharp diffraction peak at  $2\theta = 26.5^\circ$  corresponding to a layer-to-layer distance of 0.34 nm according to Bragg's law. A diffraction peak of GO appears at  $2\theta = 9.6^\circ$ , representing an interlayer spacing of 0.92 nm due to intercalation by oxygen-containing groups and moisture. **RGO** shows a broad and weak peak at  $2\theta = 26^\circ$  without appearance of the characteristic peaks at low diffraction angles, which can be ascribed to exfoliation into a monolayer or few-layers.<sup>7</sup>

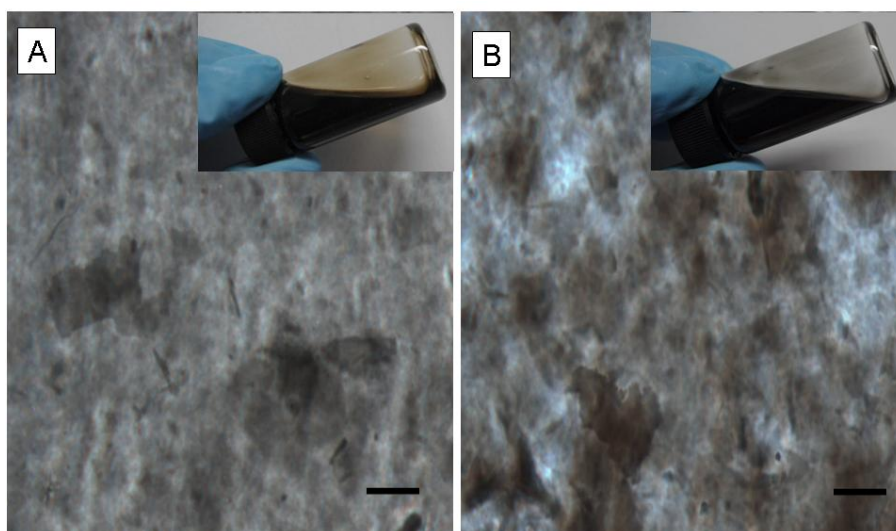


**Fig. S5** OM micrographs of 1 wt% GO/PVA (A) and RGO/PVA (B) suspensions. The scale bars represent 1  $\mu\text{m}$ . The opaque regions represent the dispersed nanosheets and the brightness is in inverse proportion to the thickness of stacked sheets. Almost homogeneous color dispersion in the OM micrographs shows that both GO and RGO nanosheets are well-dispersed in the suspensions except for only a few visible stacks attributed to the overlap of fillers. Insets show photographs of the suspensions placed statically for around 2 months. No sediment was observed at the bottom of the vials, indicating the “true solution” character for the suspensions.

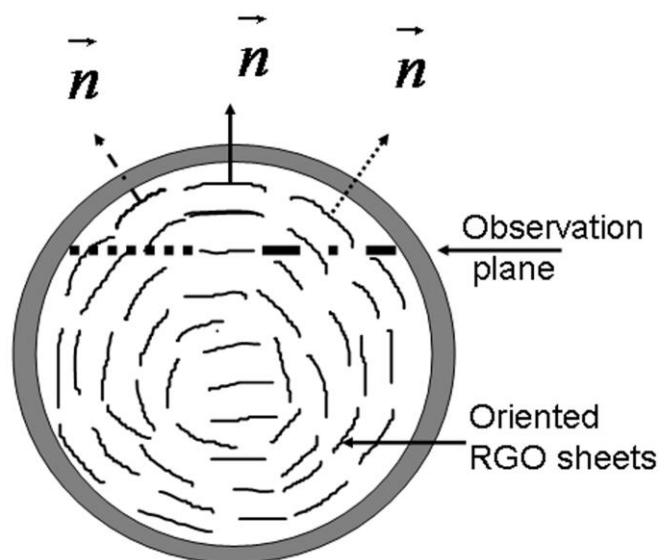


**Fig. S6** Schematic illustration of the ordered structure of RGO sheets in the in-situ shear flow capillary cell. The nanosheets are aligned with the plane parallel to the flow direction and the normal of the nanosheet plane in the diameter direction. The direction of the flow is perpendicular to the paper. The dot line and the dash and dot line represent different normal directions of sheets, and induced bright regions (birefringence), corresponding to Fig. 3D and 3E, respectively.

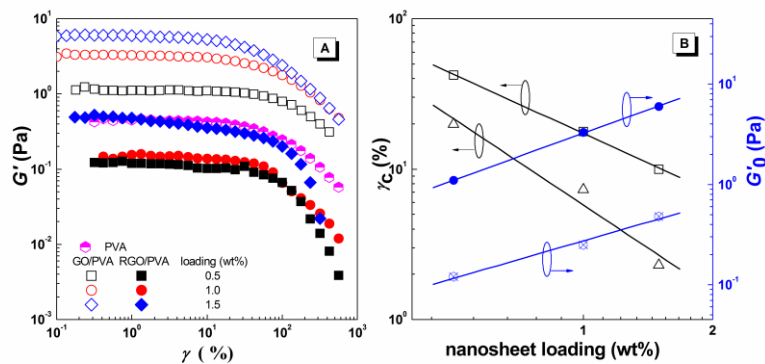


**Fig. S7** (A) Storage modulus ( $G'$ ) as a function of strain ( $\gamma$ ) for PVA solution ( $C = 10$  wt%) and the GO/PVA (hollow symbols) and RGO/PVA suspensions (solid symbols) at  $3.14$  rad  $s^{-1}$  at  $20$  °C. (B) Critical strain ( $\gamma_c$ ) and  $G'$  in the linearity region ( $G'_0$ ) as a function of GO or RGO loading.  $G'$  is constant at small  $\gamma$  whereas it dramatically decreases at the large  $\gamma$ . The rheological nonlinearity of the suspensions becomes marked with increasing nanosheet loadings, which is associated with release of trapped entanglement and breakdown of H-bondings. The variation tendency of  $G'_0$  is similar to  $\eta_{0.01}$  shown in Fig. 2B.  $G'_0$  obeys a power law dependence of  $G'_0 \sim \varphi^y$  and the value of  $y = 1.54 \pm 0.03$  for GO suspensions is significantly higher than that of  $y = 1.24 \pm 0.14$  for the RGO suspensions, which could be ascribed to more adsorption of PVA chains on the surface of GO nanosheets by interfacial H-bonding. Here,  $\varphi$  represents weight fraction of nanosheets.  $\gamma_c$  of GO/PVA suspensions is higher than that of RGO/PVA suspensions.  $\gamma_c$  also exhibits a power law dependence  $\gamma_c \sim \varphi^{-z}$  with  $z = 1.31 \pm 0.04$  and  $z = 1.90 \pm 0.37$  for GO/PVA and RGO/PVA suspensions, respectively. The lower  $z$  exponent and the high  $\gamma_c$  value of GO/PVA suspensions are attributed to strong interfacial interaction between PVA chains and GO nanosheets.

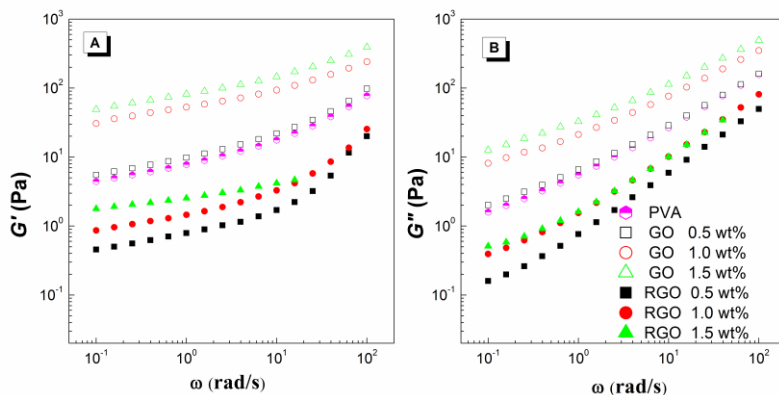


**Fig. S8** (A) Storage modulus ( $G'$ ) and (B) loss modulus ( $G''$ ) as a function of frequency ( $\omega$ ) for PVA solution ( $C = 10$  wt%) and the GO/PVA (hollow symbols) and RGO/PVA suspensions (solid symbols) at  $5$  °C.

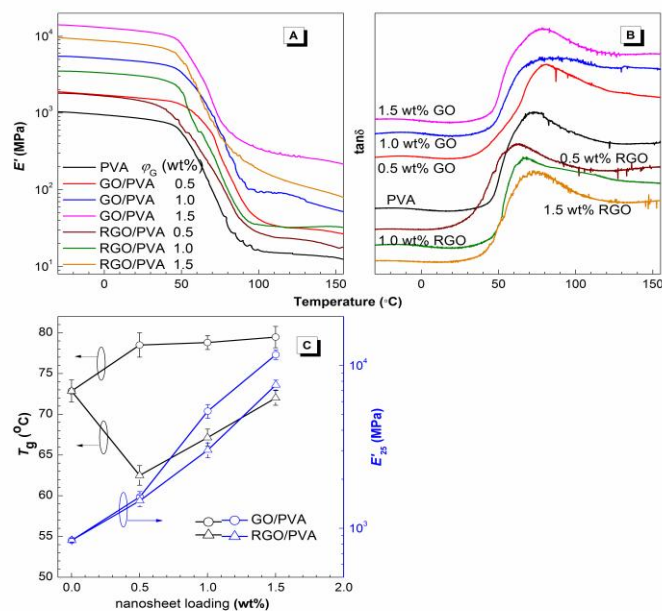


**Fig. S9** (A) Storage modulus ( $E'$ ) and (B) loss fact ( $\tan\delta$ ) as a function of temperature ( $T$ ) for PVA, GO/PVA and RGO/PVA films; (C)  $T_g$  and  $E'$  at 25 °C as a function of filler loading. The  $\tan\delta$  curves are vertically shifted by various factors. While  $E'$  increases with increasing nanosheet loading,  $E'$  of GO/PVA films is higher than that of RGO/PVA films due to the strong interfacial interaction between GO sheets and PVA chains. Starr et al.<sup>8</sup> showed an increase of  $T_g$  for polymer chains in the close vicinity of nanoparticle inclusions when an attractive potential is present. If excluded-volume interactions are present,  $T_g$  is predicted to decrease.<sup>9</sup>  $T_g$  of the film with 0.5 wt% RGO is far lower than that of PVA, ascribing to promotion of motion of chain segments by breakage of inter-chain H-bonding;  $T_g$  of the film with 0.5 wt% GO is higher than that of PVA, ascribing to the strong interfacial interaction between PVA chains and GO nanosheets.  $T_g$  of both nanocomposite films increases with further increasing nanosheet loading, which can be ascribed to nanoconfinement effect. The nanosheet filling causes an increment in  $E'$  at 25 °C and the increment in the GO/PVA film is more significant than in the RGO/PVA film.

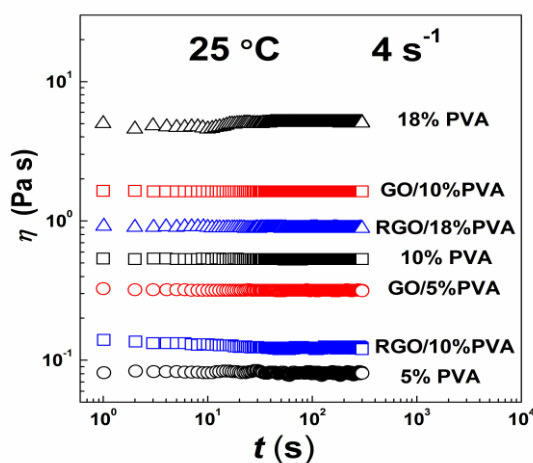


**Fig. S10** The peak hold curves of various spinning solutions.

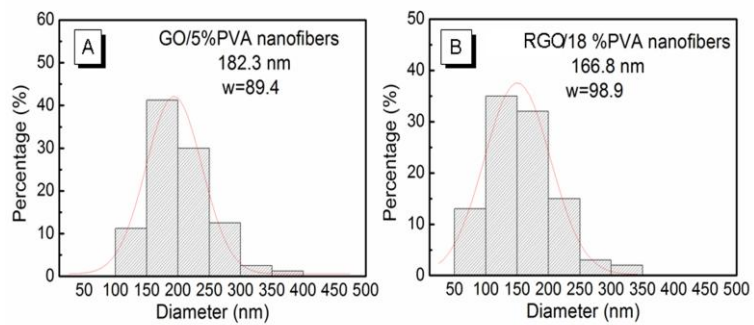


**Fig. S11** Size distribution histograms of GO/PVA nanofiber electrospun at  $C = 5$  wt% calculated from Fig. 11A2 (A) and of RGO/PVA nanofiber electrospun at  $C = 18$  wt% calculated from Fig. 11B2 (B) with the aid of Image J. The red curve is drawn according to Gaussian distribution.

**Table S1. Rheological exponents for PVA solution ( $C = 10$  wt%) and nanosheet suspensions.**

Suspensions	$x^a$	$x^b$
PVA	0.84±0.03	0.16±0.01
0.5 wt% GO	0.76±0.02	0.35±0.01
1.0 wt% GO	0.75±0.02	0.45±0.01
1.5 wt% GO	0.84±0.04	0.49±0.01
0.5 wt% RGO	0.78±0.02	0.26±0.02
1.0 wt% RGO	0.87±0.03	0.29±0.01
1.5 wt% RGO	0.79±0.01	0.39±0.02

<sup>a</sup> Strong shear thinning region; <sup>b</sup> Weak shear thinning region.

**Table S2. Viscosity values of spinning solutions and structural parameters of corresponding fibers.**

Sample	Viscosity at $4 \text{ s}^{-1}$ (Pa s) <sup>a</sup>	Diameter (nm)	Half- peak width (nm) <sup>b</sup>
10 wt% PVA	0.53±0.02	241.3	124.1
GO/10 wt%PVA	1.62±0.03	221.3	62.4
RGO/10 wt%PVA	0.12±0.01	121.7	89.8
5 wt%PVA	0.08±0.01	-- <sup>c</sup>	-- <sup>c</sup>
GO/5 wt%PVA	0.32±0.01	182.3	89.4
18 wt%PVA	5.05±0.03	-- <sup>c</sup>	-- <sup>c</sup>
RGO/18 wt%PVA	0.88±0.02	166.8	98.9

<sup>a</sup> The average of viscosity achieving equilibrium; <sup>b</sup> Gaussian distribution; <sup>c</sup> few nanofibers is obtained.

## Reference

- 1 W. S. Hummers and R. E. Offeman, *J. Am. Chem. Soc.*, **1958**, *80*, 1339-1339.
- 2 Z. Xu and C. Gao, *Macromolecules*, **2010**, *43*, 6716-6723.
- 3 X. Zhao, Q. H. Zhang and D. J. Chen, *Macromolecules*, **2010**, *43*, 2357-2363.
- 4 S. Stankovich, D. A. Dikin, R. D. Piner, K. A. Kohlhaas, A. Kleinhammes, Y. Jia, Y. Wu, S. T. Nguyen and R. S. Ruoff, *Carbon*, **2007**, *45*, 1558-1565.
- 5 M. S. Dresselhaus, G. Dresselhaus, A. Jorio, F. A. G. Souza and R. Saito, *Carbon*, **2002**, *40*, 2043-2061.
- 6 J. Gao, F. Liu, Y. L. Liu, N. Ma, Z. Q. Wang and X. Zhang, *Chem. Mater.*, **2010**, *22*, 2213-2218.
- 7 S. Wang, Y. Zhang, N. Abidi and L. Cabrales, *Langmuir*, **2009**, *25*, 11078-11081.
- 8 F. W. Starr, T. B. Schröder and S. C. Glotzer, *Macromolecules*, **2002**, *35*, 4481-4492.
- 9 M. E. Mackay, T. T. Dao, A. Tuteja, D. L. Ho, B. van Horn, H. C. Kim and C. J. Hawker, *Nat. Mater.*, **2003**, *2*, 762-766.